*Presented at the 35th European PV Solar Energy Conference and Exhibition, 24-28 September 2018, Brussels, Belgium*

# ANALYSIS OF GRAIN-SIZE DISTRIBUTION AND YIELD STRENGTH OF INTERCONNECTOR RIBBONS AND WIRES AT DIFFERENT STRETCHING CONDITIONS USING COLOR ETCHING

Johann Walter, Jonas Stegmaier, Achim Kraft* and Ulrich Eitner
Fraunhofer Institute for Solar Energy Systems ISE, Heidenhofstraße 2, 79110 Freiburg, Germany
*Phone: +49 761 4588 5544, E-Mail: achim.kraft@ise.fraunhofer.de

ABSTRACT: In this paper we analyze the microstructure of solder coated copper ribbon and wire interconnectors for silicon solar cells from different manufacturers at different stretch levels in longitudinal and cross microsections by color etching and microscopy. The used etchant colors each grain according to its crystallographic orientation. This enables the extraction of the grain size and frequency information by image and data processing tools. Furthermore we measure the yield strength of the solar cell interconnectors for strain levels of 0.5 %, 5 % and 10 % and evaluate the impact on the microstructure of the interconnector.
We find a large variation in the copper microstructure, especially for wires and observe an inverse relation between yield strength and grain sizes corresponding to the Hall-Petch relation. The lowest measured yield strength for a wire interconnector is about 82 MPa (avg. grain size: 237 µm²), which is about 20 MPa higher compared to the lowest yield strength measured for ribbons (avg. grain size: 247 µm²). The wire with the highest yield strength of 148 MPa shows fine grains (avg. grain size: 29 µm²). In the ribbon analysis we find the same overall correlation between grain size and yield strength with some exceptions. This underlines that grain size distribution is not the only attribute which affects the yield strength. The analysis of copper ribbons at different stretch levels discloses a deformation or refinement of the copper grains associated with rising yield strength.
In general the results show that the approach of a color etching, optimized for solar cell interconnector cross and longitudinal sections, is a suitable, fast and cost-effective solution to quantify the grain size distribution and evaluate mechanical impacts like stretching or bending on the copper microstructure.

Keywords: Copper, Color Etching, Solar Cell Interconnector, Grain, Manufacturing and Processing

## 1 INTRODUCTION

According to the common practice, silicon solar cells are interconnected by 4-5 copper ribbons or 12-15 copper wires. The interconnectors consists of a copper core coated with solder (Sn60Pb40 is widely used). For five busbar interconnection the ribbon dimensions are typically 0.22 x 0.9 mm. For multi-wire interconnection wires with a diameter between 300 µm and 400 µm are used. To reduce mechanical stress in solder joints of interconnected solar cells, caused by the CTE mismatch between silicon ($\alpha_{Si} = 2.6 \cdot 10^{-6}$ $K^{-1}$) [1] and copper ($\alpha_{Cu} = 17.0 \cdot 10^{-6}$ $K^{-1}$) [2], the use of soft interconnectors with low yield strength is recommended [3-4]. The yield strength is strongly influenced by the manufacturing process of the copper interconnector resulting in different bulk material structures [5-6]. Typical yield strength values are around 60 MPa for ribbons and 80 MPa for wires. Before interconnecting the solar cells by soldering in a stringer the interconnectors are typically pre-stretched to enable a precise alignment to the solar cell.

In this work we investigate the copper grain structure of ribbons and wires with different yield strengths and at different stretching modes by color etching of metallographic cross and longitudinal sections prepared similar to literature [7].

Color etching, also called tint etching or stain etching, has been known for almost 100 years [8]. Many different reagents, called tint etchants or color etchants, were developed for different selective materials [9-11], such as copper [2,12] or alloy phases [13]. During the color etching process a stable fine film is deposited at the microsection surface [14]. The thickness varies for different grains depending on its crystallographic orientation. Due to interference effects these grains appear in different colors in the microscope image.

Due to improvements in image processing in the last decade, advanced tools and algorithms allow an efficient and quantitative analysis of color etched images and enable the examination of grain size information. Color etching enables a very fast grain boundary scanning of large areas making the technique a promising approach for the analysis of grain size distributions of solar cell interconnectors.

## 2 EXPERIMENTAL APPROACH

In this study we analyze ribbons and wires, in terms of yield strength and copper microstructure. The interconnectors are pre-stretched and the impact on grain size and yield strength is investigated.

A precise and reproducible pre-stretching of the solar cell interconnectors, as well as the determination of the yield strength is performed using a tensile tester according to ISO 6892-1 [15]. Table I shows the interconnector configurations and measured yield strength data. The interconnectors vary in cross section area, manufacturer (A – D) and initial yield strength. In terms of mechanical stress a low yield strength is beneficial for the interconnection of solar cells [3].

**Table I:** Measured yield strength of ribbon and wire interconnectors for different pre-stretching modes.

| Pre-stretching mode [%] | | Initial state | 0.5 | 5.0 | 10.0 |
|---|---|---|---|---|---|
| | Mfr. | Yield strength [MPa] | | | |
| Ribbon R1 (0.2 x 1.5 mm²) | A | 61.1 | 68.8 | 137.5 | 182.3 |
| Ribbon R2 (0.2 x 1.5 mm²) | B | 65.3 | 73.4 | 136.3 | 178.2 |
| Ribbon R3 (0.2 x 1.0 mm²) | B | 75.7 | 83.9 | 146.7 | 190.0 |
| Ribbon R4 (0.22 x 0.9 mm²) | C | 78.0 | 85.6 | 145.7 | 186.5 |
| Ribbon R5 (0.18 x 1.0 mm²) | C | 110.0 | 117.6 | 162.2 | 193.6 |
| Ribbon R6 (0.06 x 1.5 mm²) | C | 163.8 | 171.2 | 218.2 | 248.5 |
| Wire W1 (Ø = 350 µm) | A | 81.9 | 89.4 | 165.5 | 203.5 |
| Wire W2 (Ø = 350 µm) | B | 106.7 | 112.6 | 164.1 | 198.4 |
| Wire W3 (Ø = 300 µm) | D | 148.1 | 158.2 | 201.6 | 231.9 |

We analyze the grain boundary by means of an optimized color etching process. For each sample group, we cut six randomized 20 mm pieces out of one 1.2 m interconnector strip for color etching. In this way we ensure to cover a large variety of microstructures within the interconnector in our analysis.

Figure 1 shows the process steps. After the very last very fine polishing, color etching is applied to the samples and a high resolution image is captured by digital microscopy. The image is analyzed by software to extract the grain boundary size of each grain. An algorithm detects the grain boundaries. Subsequently, the data are processed to enable a comparison of grain size distribution. Figure 1d) shows the cumulative relative grain area (a) and the cumulative relative frequency (f) for four different cross sections of one interconnector. For the analysis of the frequency a bin size of 0.2 µm$^2$ is used. Since the cumulative area curves often show a higher deviation, especially for larger grain sizes, we recommend to use the frequency for comparison of different interconnectors. In the result diagrams we show the averages of 3 to 6 curves for each interconnector (figure 1e). The number of evaluated samples depends on the quality of the obtained etched surfaces. Etching quality varies across samples and depends mainly on factors such as evenness, polishing, impurities, oxidation or etching process stability. All samples in one group are etched simultaneously.

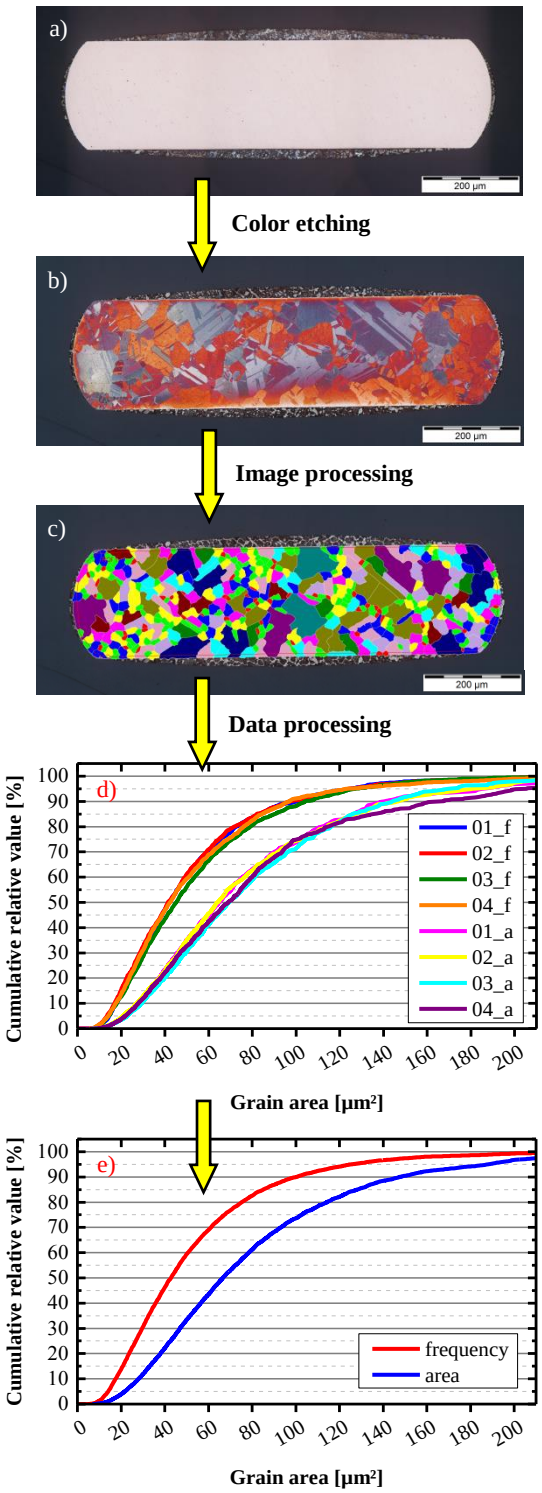


**Figure 1:** Microscope image of the metallographic cross section of a ribbon after grinding and polishing a), after color etching revealing the grain structure of the interconnector copper material b), after image processing c). The relative area as well as the relative frequency (bin = 0.2 µm²) of all grains are plotted cumulatively over the full grain boundary range d). By cumulating the values, the differences between interconnectors are more clearly visible. Curves are averaged respectively for area and frequency e).

## 3 RESULTS

### 3.1 Color etching

One representative color etched overview and detail image of each interconnector sample (cf. table I) at initial state (non-stretched) is shown in figure 2 to figure 10. The detail images show the magnified microstructure of the yellow highlighted sections in the overview image. Due to the nature of color etching, it is not possible to compare colors between images. The color result depends on parameters such as temperature, etching time, concentration of the color etchants, microstructure and polishing. Slight deviation can lead to different colors. However, the variety of colors gives an idea of the homogeneity in grain orientation since identical colors represents identical orientation within the sample. However for copper the orientation {100} is favored [16]. To extract the grain orientation information, methods such as electron backscatter diffraction (EBSD) can be used.

Depending on the manufacturing process the interconnectors are treated differently (temperature profile, system etc.). This is reflected by the differences in microstructure. In general, flat ribbon interconnectors are drawn, rolled flat, annealed and solder coated [17]. For example, the 60 µm thick ribbon R6 (figure 7) shows small grains (avg. grains: 53 µm²), whereas the grains for the 220 µm thick ribbon R4 (figure 5) are significantly larger (avg. grains: 247 µm²). Both ribbons are from the same manufacturer (table II). For wire W1 (figure 8) the color etching reveals very large grains whereas for wire W2 (figure 9) we observe larger grains in the center and smaller grains all around the edges. Wire W3 (figure 10) shows overall very small grains. Further analyses are shown in chapter 3.3.

We assume in case of very fine grain sizes that there might be some issues in the annealing process (temperature profile, interconnector transport) especially for wires because of their less mechanical resilience to deformation and less copper material. This correlates also with the fact that manufacturers have issues to achieve yield strength about 60 MPa for wires (cf. table I, manufacturer A).

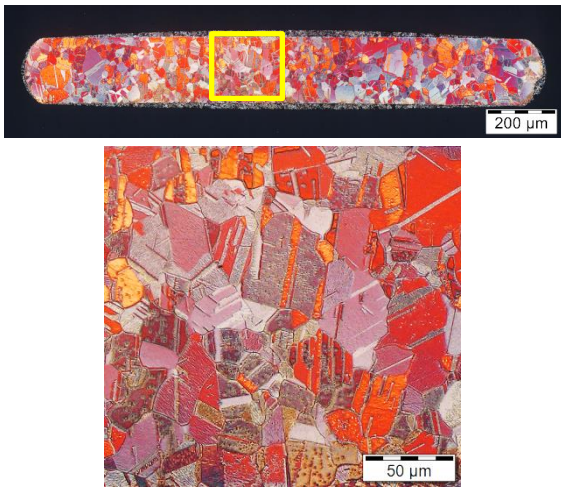


**Figure 2**: Ribbon R1 (0.2 x 1.5 mm²), manufacturer A


**Figure 3:** Ribbon R2 (0.2x1.5 mm²), manufacturer B

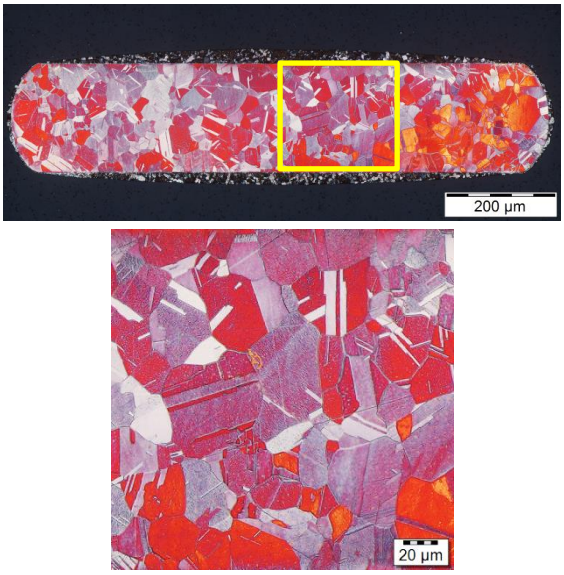


**Figure 4:** R3 (0.2x1.0 mm²), manufacturer B

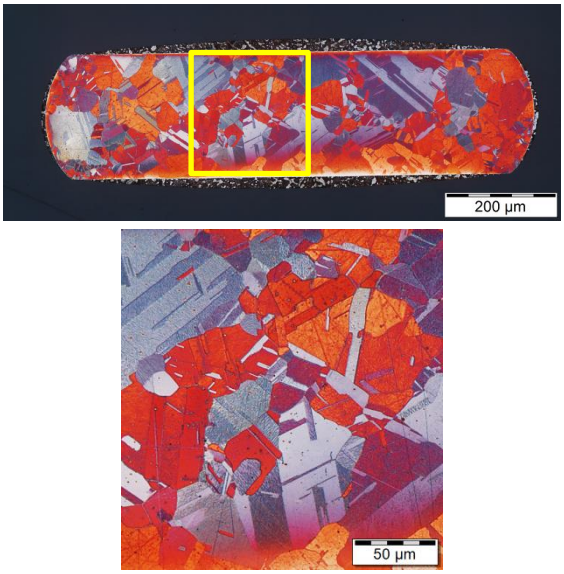


**Figure 5:** R4 (0.22 x 0.9 mm²), manufacturer C

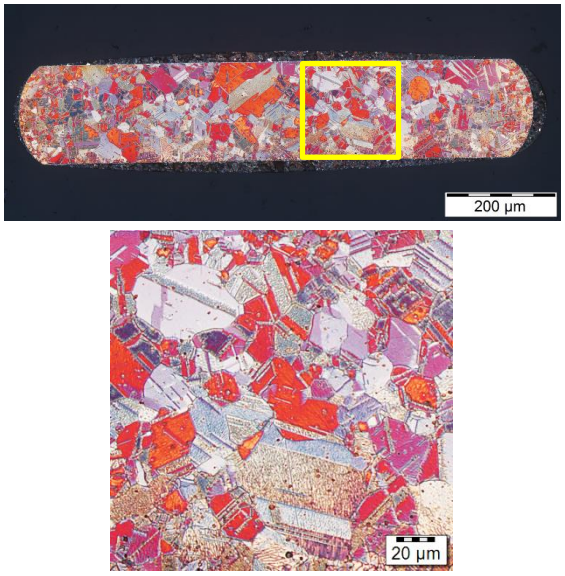


**Figure 6:** R5 (0.18 x 1.0 mm²), manufacturer C

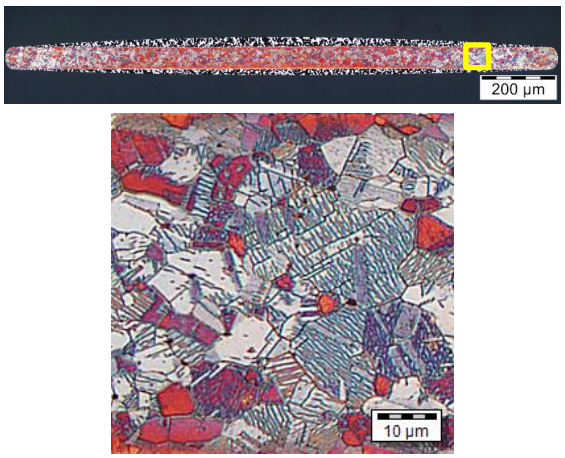


**Figure 7:** R6 (0.06 x 1.5 mm²), manufacturer C

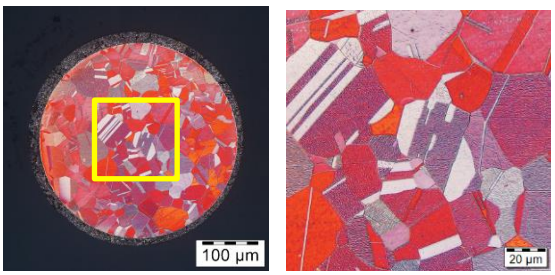


**Figure 8:** W1 (Ø =350 µm), manufacturer A

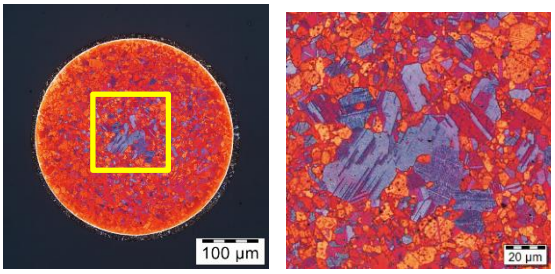


**Figure 9**: W2 (Ø =350 µm), manufacturer B

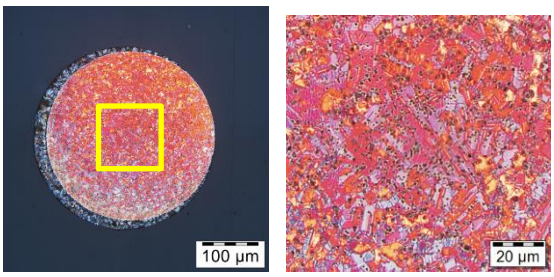


**Figure 10:** W3 (Ø =300 µm), manufacturer D. The black dots represent polishing artefacts.

3.2 Influence of stretching modes on microstructure

We apply the presented method (figure 1) to evaluate the grain size distribution of the interconnectors at initial state and after stretching. Figure 11 shows the deviation within a group of wire sample W3 non-stretched (initial state) and after 10 % stretching. In this case each group consists of four samples. The variation within a group is less than 5 $\%_{absolute}$. In general color etching shows a good agreement with the grain size distribution determined by EBSD [18].

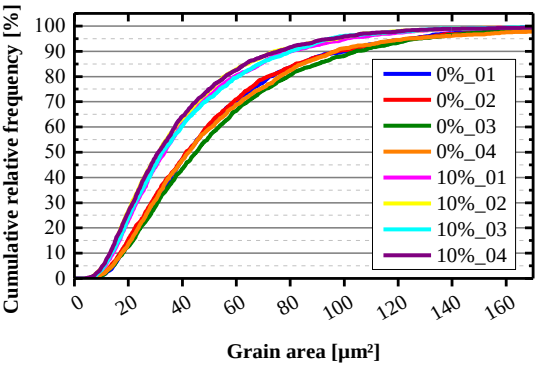


**Figure 11:** Grain size results after color etching and data processing of four samples (W3) non-stretched and after 10% stretching. The deviation is less than 5 $\%_{absolute}$ within each group.

For the ribbons, besides the cross section the longitudinal section is evaluated as well. A detailed strain analysis with color etching and determination of grain size distribution is exemplarily shown for ribbon R4 und wire W3 (figure 12 – figure 17). Due to the round shape of the wires it is not possible to polish the samples to the same longitudinal position within a group. This has a significant impact on the evaluated area and the results due to very inhomogeneous grain size distributions in the cross section e.g. center and edge. For this reason, we do not perform the analysis of longitudinal sections for wires.

**Microsection of ribbon R4 (longitudinal section)**

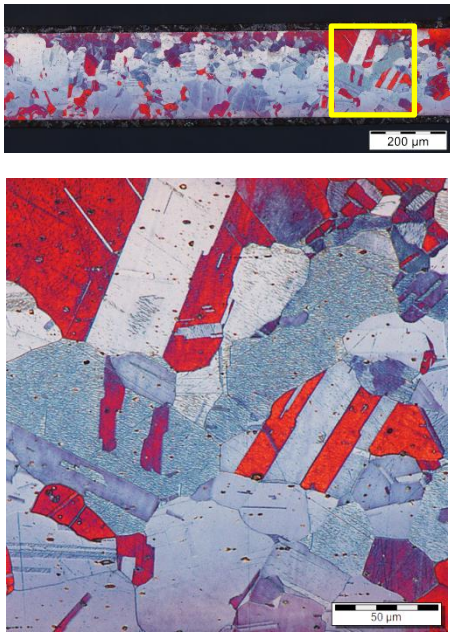


**Figure 12:** Half size of the captured longitudinal section and detailed image of ribbon R4, without pre-stretching ($R_{p0.2}$ = 163.8 MPa).

**Data processing ribbon R4 (longitudinal section)**

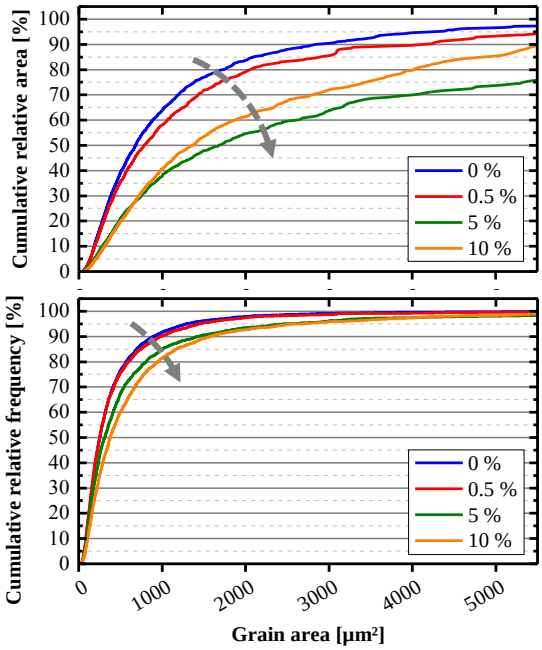


**Figure 14:** Distribution of grains of ribbon R4 (longitudinal section). The arrows indicated the change direction in grain distribution due to stretching.

**Microsection of ribbon R4 (cross section)**

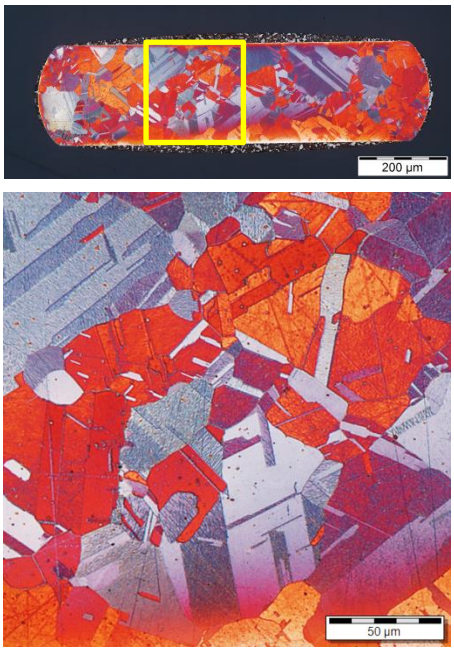


**Figure 13:** Cross section and detailed image of ribbon R4 after 0.5 % pre-stretching ($R_{p0.2}$ = 171.2 MPa).

**Data processing ribbon R4 (cross section)**

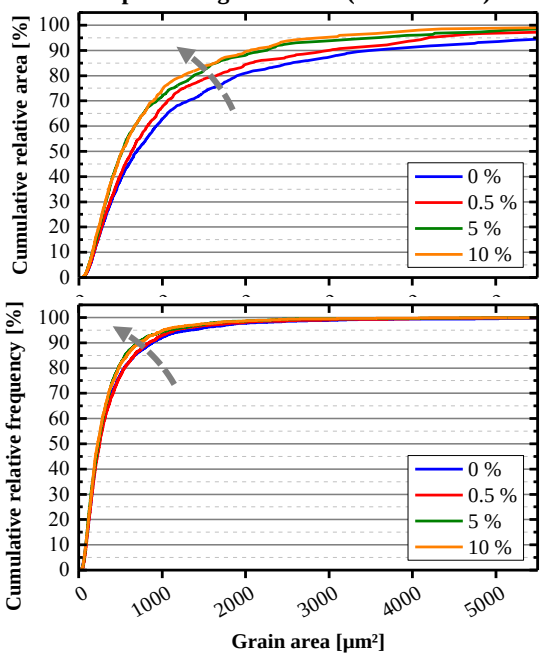


**Figure 15:** Distribution of grains of ribbon R4 cross section. The arrows indicated the change direction in grain distribution due to stretching.

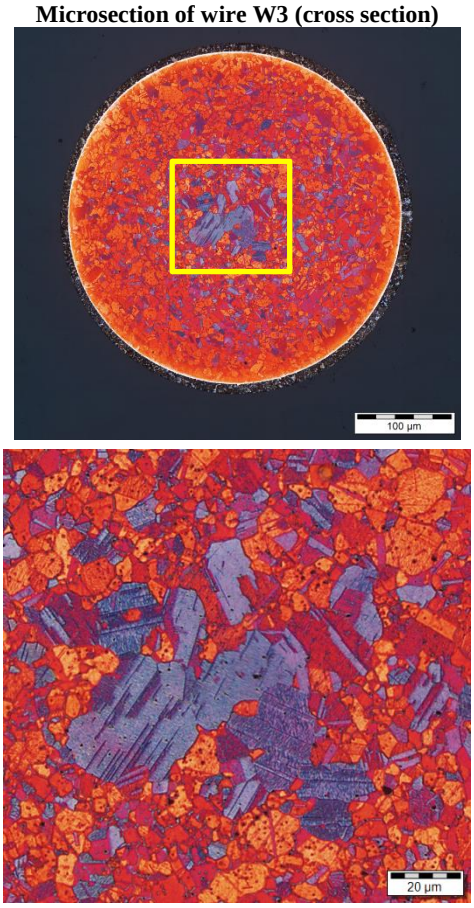


**Figure 16:** Cross section and detailed image of wire W3 after 0.5% pre-stretching ($R_{p0.2}$ = 158.2 MPa).

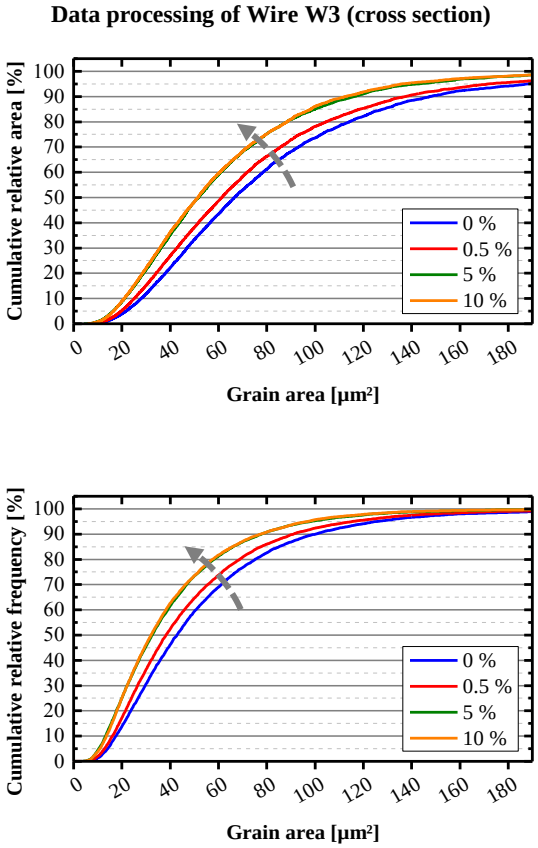


**Figure 17:** Distribution of grains of wire W3 cross section. The arrows indicated the change direction in grain distribution due to stretching.

Figure 14, 15 and 17 show the results after image and data processing of the color etched images (procedure cf. figure 1). Each curve represents the mean value of 3 - 6 evaluated microsections. The number of detected grains within a batch varies between 2.000 - 10.000 grains depending on the sample. The curves showing the relative area distribution present the area proportions of different grain sizes. The 50% threshold means 50 % of the area is covered by grains of the given grain sizes. Larger grains result in a flatter appearance of the curve.

Furthermore the curves show the cumulative relative frequency. This gives information about the frequency proportion of different grain sizes (bin size: 0.2 µm² grain area). A higher number of grains within the same grain bin leads to a steeper shape of the curve. A very similar number of grains of each grain size would result in a linear curve. The 50% threshold represents the median.

According to the cross section data both evaluated samples, ribbon R4 and wire W3, indicate a drift to smaller grains with increased pre-stretching.

In the longitudinal section analysis, higher pre-stretching levels result in larger grains. The curves become flatter (figure 14). The grain size appears smaller in cross sections but larger in the longitudinal sections. It seems that larger grains get deformed or refined into smaller ones during stretching. This explains the increased frequency for smaller grains. Due to literature stretching is most likely [19] but has to be investigated on further. For 0 % and 0.5 % stretching the grain size change seem to be too low to detect any difference.

### 3.3 Analysis of yield strength and different grain size distributions at initial state.

Based on the method as shown in figure 1 we analyze the microstructure of different ribbon and wires at initial state and calculate the cumulative relative frequency curves (figure 18 and figure 20) and the non-cumulative frequency curves (figure 19 and figure 21) for every group.

As shown in figure 14 and figure 15, stretching the grains of ribbon R4 does not e.g. doubling or halving any values in the grain size distribution curves, although the yield strength increases by a factor of 2.4 after 10 % stretching (table I). This means, grain size and yield strength does not change with same dynamic due to stretching. However, figure 18 to figure 21 disclose that the manufacturing process has a large impact on the grain size distribution curves.

Figure 19 shows that the relative frequency peak of W1 (81.9 MPa) is shifting from 52.2 µm² grain area to 15 µm² for W3 (148.1 MPa). The average grain size is changing from 237 µm² for W1 to 29 µm² for W3 (table II).

In figure 18 we observe a steeper curve shape with increasing yield strength. In figure 20 the same behavior can be observed for the ribbons R1 (61.1 MPa), R2 (65.3 MPa), R5 (110.0 MPa) and R6 (163.8 MPa).

R3 (75.7 MPa) and R4 (78.0 MPa) have larger grains compared to R1 and R2 but we measure a 10 - 20 MPa higher yield strength. This correlation is also confirmed by the average grain sizes in table II. These differences are caused by the fact that the yield strength depends not only on grain size, but also on material properties such as impurities, dislocations or grain orientation [20-21].

The grain size distribution is correlated to yield strength but its not the only influence parameter. We also find that different interconnector types, such as ribbon or wires, can not be compared directly since the resulting curve shape differs significantly for similar yield strengths as displayed for W2 and R5. However, for most of the interconnectors, we observe that larger grains result in lower yield strength, which is also proclaimed by the Hall-Petch relation [22-23]. It predicts a linear dependence of the yield strength or hardness on the average grain size ($\sigma_{\text{yield stress}} \sim D_{\text{grain size}}^{-1/2}$) [24]. With decreasing grain size less dislocation slipping can happen as the grain boundary represents an obstacle [25]. Since dislocation slipping is necessary for plastic deformation, material with smaller grains becomes harder, resulting in higher yield strength. Although grain refinement is not useful for interconnectors it is a typical technique for strengthening a material [26-27].

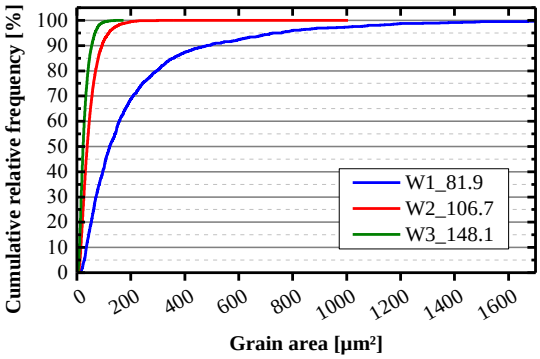


**Figure 18:** Distribution of the grain sizes at initial state of three different wires with different yield strength (cumulative).

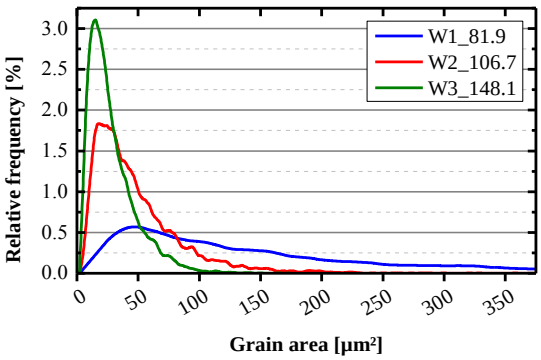


**Figure 19:** Distribution of the grain sizes at initial state of three different wires with different yield strength (relative).

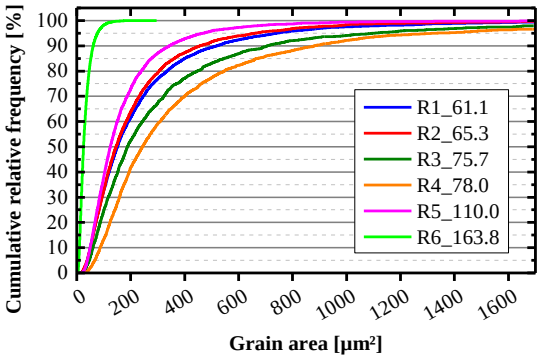


**Figure 20:** Distribution of the grain sizes at initial state of six different ribbons with different yield strength (cumulative).

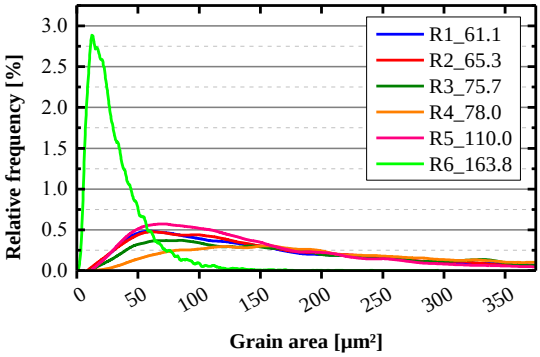


**Figure 21:** Distribution of the grain sizes at initial state of six different ribbons with different yield strength (relative).

**Table II:** Average grain size data after image and data processing from different non-stretched interconnectors and manufacturers.

| | Mfr. | Initial yield strength [MPa] | Avg. grain size [µm²] |
|---|---|---|---|
| Ribbon R1 (0.2 x 1.5 mm²) | A | 61.1 | 247 |
| Ribbon R2 (0.2 x 1.5 mm²) | B | 65.3 | 238 |
| Ribbon R3 (0.2 x 1.0 mm²) | B | 75.7 | 332 |
| Ribbon R4 (0.22 x 0.9 mm²) | C | 78.0 | 452 |
| Ribbon R5 (0.18 x 1.0 mm²) | C | 110.0 | 174 |
| Ribbon R6 (0.06 x 1.5 mm²) | C | 163.8 | 53 |
| Wire W1 (Ø = 350 µm) | A | 81.9 | 237 |
| Wire W2 (Ø = 350 µm) | B | 106.7 | 50 |
| Wire W3 (Ø = 300 µm) | D | 148.1 | 29 |

3.4 Analysis on wave-shaped interconnector

Wave shaped interconnectors, which are beneficial for low mechanical stress in solder joints [3], can also be analyzed by color etching. During the shaping process the grains get crushed in the inner radius and stretched with increasing radius as displayed in figure 22. On the one

hand wave shaping lowers the effective yield strength [28] but on the other hand the process results in unfavorable mechanical properties in the bended area. Further analyses on this issue to enhance the bending process are in progress.

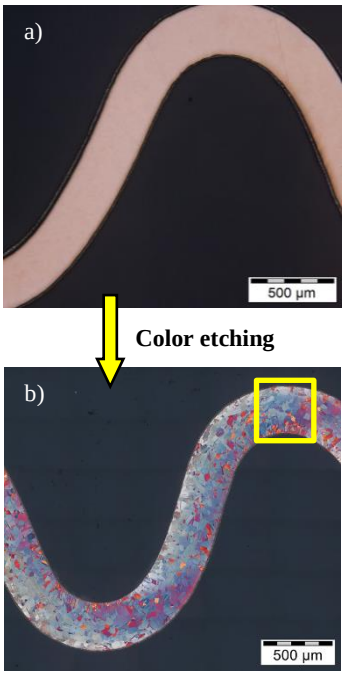


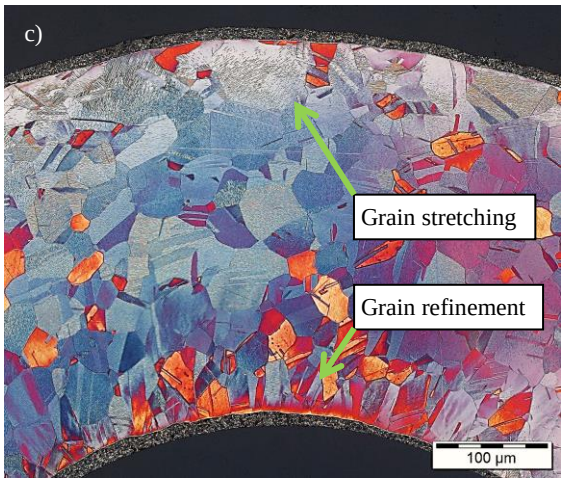


**Figure 22:** Longitudinal section of an interconnector revealing grain boundary deformation due to wave shaping. a): Original longitudinal section of a wave shaped interconnector. b): Wave shaped interconnector after color etching. c) Detailed view of the in b) highlighted bent area.

## 4 CONCLUSION

In this paper we analyze the grain boundary structure of 6 different ribbons and 3 different wires for solar cell interconnection by an optimized color etching process. The samples come from different manufacturers and vary in their initial yield strength and geometry. We analyzed them at non-strained and different strain levels and we complement the results with yield strength measurements. Color etching reveals the microstructure of the copper core of the ribbon by coloring the crystallographic orientation of each grain which is studied in longitudinal and cross microsections.

Compared to other methods - such as EBSD or LabDCT - color etching, combined with microscopy, delivers very fast grain boundary information of large areas, which can be used to extract the grain size distribution by image and data processing. The largest evaluated microstructure in our study is about 2270 x 220 µm². Typical etching times are within a few minutes. As the absolute color result is strongly dependent on the parameters of each individual sample (microstructure, temperature, color etchants concentration, etching time, etc.), quantitative color comparison across different samples is not possible. However, since identical colors represent identical grain orientation within a sample, knowledge about grain orientation homogeneity can be delivered but the exact orientation is unknown.

We showed that the grain size deviation of samples within the same group is < 5 % which is an acceptable variation for the purpose of this study. The strongest influence is the etching quality which depends on the copper surface quality (evenness, polishing, impurities, oxidation or etching process stability). For the analysis we recommend to use the frequency curves instead of the area curves since large single grains, which sometimes occur in samples, have a significant impact on the area curves, resulting in a stronger curve deviation at larger grains, but hardly affect the frequency curves.

The analyzed wires show a correlation between yield strength and grain sizes distribution, similar to the Hall-Petch relation, which expects microstructures with large grains to have a lower yield strength (table II bottom). W1 (82 MPa) has the largest grains (figure 8) and lowest yield strength (table I). W2 (107 MPa) has large grains in the center and small grains all around the edge (figure 9). W3 (148 MPa) has evenly distributed small grains (figure 10). This relation is also shown in the frequency curves (figure 18). However, for the ribbons we find the same overall tendency but also observe that yield strength is not only dominated by grain size. R3 and R4 have overall larger grains but a 10 -20 MPa higher yield strength compared to R1 and R2 (table II top). We assume this might be related to differences in grain orientation, dislocations or impurities, which also affect yield strength [20-21] and for which our color etching method is not sensitive. The highest yield strength is measured for R6 (164 MPa) which also exhibits the smallest thickness (60 µm) and smallest grains. It is notable that the lowest ribbon yield strength is about 60 MPa and for wires it is about 80 MPa. As the low yield strength for ribbons has been requested by the PV industry and is an established feature of solar ribbons today our analysis indicates that there might be optimization potential for processing round-shaped wires for an application in PV.

Stretching enlarges the grains in the longitudinal direction and reduces the grain size in the normal plane direction. The reduction of grain size is either caused by grain refinement or grain deformation. Due to the cold hardening the yield strength increases. For ribbon R4 at 10 % strain level (187 MPa) the yield strength raises by a factor of 2.4. The influence of stretching is also visible on grain size level in the longitudinal (figure 14) and cross

sections (figure 15) for ribbon R4. Due to stretching not only the grain size but also the grain orientation can change [19] which cannot be detected by color etching. For this reason we suggest using this method on interconnectors in their initial state only, as differences in the manufacturing process can be observed easily (figure 18, figure 20, table II).

Our study shows that color etching is a suitable, fast and cost-effective alternative to reveal the copper microstructure of solar cell interconnectors and analysis of grain sizes and frequency over a large area.

ACKNOWLEDGEMENTS

This work has been supported by the Federal Ministry for Economic Affairs and Energy under the contract number 0324057B, acronym BACKBONE.

REFERENCES

[1] K. G. Lyon, G. L. Salinger, C. A. Swenson, and G. K. White, "Linear thermal expansion measurements on silicon from 6 to 340 K", Journal of Applied Physics, vol. 48, no. 3, 1977, pp. 865-868, doi: 10.1063/1.323747

[2] J. R. Davis, "Copper and copper alloys", ASM International, 2001, ISBN: 0-87170-726-8.

[3] R. Meier, M. Pander, R. Klengel, S. Dietrich, S. Klengel, M. Ebert, and J. Bagdahn, "Reduction of soldering induced stresses in solar cells by microstructural optimization of copper-ribbons", Proceedings of Society of Photographic Instrumentation Engineers, vol. 811206, 2011, pp. 1-13, doi: 10.1117/12.893519.

[4] B. Kang N. Park, S. J. Tark, W. W. Oh, S. Park, Y. D. Kim, H. Lee, and D. Kim, "Advanced yield strength of interconnector ribbon for photovoltaic module using crystallographic texture control", vol. 20, no. 2, 2014, pp. 229-232, doi: 10.1007/s12540-014-2005-x.

[5] A. Butz, D. Helm, and R. Meier, "Microstructural analysis and process chain simulation of copper-ribbons for solar cell Interconnections", 8th European Solid Mechanics Conference, 2012.

[6] A. Butz, R. Meier, and D. Helm, "Simulationsbasierte Untersuchung der Eigenschaften von Bauteilen aus Kupfer am Beispiel der Fertigungskette von Solarzellenverbindern", Metall, vol. 3, 2012, pp. 28-31.

[7] D. Eberlein, P. Schmitt, and P. Voos, "Metallographic solder preparation of soldered solar cells", Practical Metallography, vol. 48, 2011, pp. 402-408.

[8] H. S. Rawdon, and M. G. Lorentz, "Metallographic etching reagents", National Bureau of Standards, vol. 16, 1920.

[9] G. Pestrow, "Metallographic etching: techniques for metallotraphy, ceramography, plastography", ASM International, 1999, ISBN: 978-0871706331.

[10] G. F. Vander Voort, "Metallography and microstructures", vol. 9, ASM International, 2004, pp. 493-512, ISBN: 978-0-87170-706-2.

[11] E. Weck, and E. Leistner, "Metallographic instructions for colour etching by immersion", Deutscher Verband für Schweißen und verwandte Verfahren, vol. 2, 1995, ISBN: 978-3-87155-146-8.

[12] G. F. Vander Voort, "Copper color metallography", Advanced Materials & Process, vol. 158, no. 1, 2000, pp. 36-40.

[13] G. F. Vander Voort, "Color metallography", Microscopy Today, vol. 13, no. 6, 2005, pp. 22-27.

[14] G. F. Vander Voort, "Metallography: principles and practice", ASM International, 1984, reprinted by ASM International, 1999, ISBN: 978-0871706720.

[15] ISO 6892-1, "Metallic materials - Tensile Testing", 2009.

[16] D. P. Field, "Metallography and microstructures", vol. 9, ASM International, 2004, pp. 215-226, ISBN: 978-0-87170-706-2.

[17] R. Meier, M. Pander, S. Großer, and S. Dietrich, "Microstructural optimization approach of solar cell interconnectors fatigue behavior for enhanced module lifetime in extreme climates", Energy Procedia, vol. 92, 2016, pp. 560-568, doi: 10.1016/j.egypro.2016.07.020.

[18] T. Bernthaler, and G. Schneider, "Fortschritte in der Metallographie", Deutsche Gesellschaft für Materialkunde, 51. Metallographie-Tagung, 2017, pp. 79-84, ISBN: 978-3-88355-415-0.

[19] H. Oettel, and H. Schumann, „Metallografie: Mit einer Einführung in die Keramografie", Wiley-VCH Verlag, vol. 15, 2011, ISBN: 978-3527322572.

[20] J. Rösler, H. Harders, and M. Bäker: "Mechanisches Verhalten der Werkstoffe", Springer Vieweg, vol. 4, 2012, ISBN: 978-3835102408.

[21] B. V. Petukhov, "A Theory of the Effect of Impurities on the Yield Stress of Silicon Crystals", Semiconductors, vol. 38, no. 4, 2004, pp. 369-375.

[22] E. O. Hall, "The deformation and ageing of mild steel", Proceedings of the Physical Society, section B, vol. 64, 1951, pp. 747-753, doi: 10.1088/0370-1301/64/6/305.

[23] N. J. Petch, "The cleavage strength of polycrystals", Journal of the Iron and Steel Institute, vol. 174, 1953, pp. 25-28.

[24] M. A. Meyers, and K. K. Chawla, "Mechanical behavior of materials", Prentice Hall, 2009, ISBN: 978-0131395060.

[25] J. Schiotz, "Simulations of nanocrystalline metals at the atomic scale. What can we do? What can we trust?", Science of Metastable and Nanocrystalline Alloys, 2001, pp. 127-139, ISBN: 87-550-2916-7.

[26] C. M. L. James, "Mechanical properties of nanocrystalline materials", CRC Press, vol 51, no. 4, 2006, pp.133-162, ISBN: 978-9814241977.

[27] E. Arzt, "Size effects in materials due to microstructural and dimensional constraints: a comparative review", Acta Materialia, vol. 46, no. 16, 1998, pp. 5611-5626, doi: 10.1016/S1359-6454(98)00231-6.

[28] J. Walter, L. C. Rendler, A. Halm, V. Mihailetchi, A. Kraft, and U. Eitner, "Ribbon interconnection of 6'' BC-BJ solar cells", Energy Procedia, vol. 124, 2017, pp. 504-514, doi: 10.1016/j.egypro.2017.09.287.